Phys. Rev. B **80**, 075403:1-6 (2009) http://dx.doi.org/10.1103/PhysRevB.80.075403

Significant Negative Differential Resistance Predicted in Scanning Tunneling Spectroscopy for a C_{60} Monolayer on a Metal Surface

X.Q. Shi,[1] Woei Wu Pai,[2] X.D. Xiao,[3] J.I. Cerdá,[4] R.Q. Zhang[1], C. Minot[1,5] and M.A. Van Hove[1,*]

[1] Department of Physics and Materials Science, City University of Hong Kong, Kowloon, Hong Kong SAR, China

[2] Center for Condensed Matter Sciences, National Taiwan University, Taipei 106, Taiwan

[3] Department of Physics, Chinese University of Hong Kong, Shatin, Hong Kong SAR, China

[4] ICMM-CSIC, Cantoblanco, 28049 Madrid, Spain

[5] Laboratoire de Chimie Théorique, UMR7616, Université P. et M. Curie-Paris 6, 4 Place Jussieu case 137, 75252 Paris Cedex 05, France

Receipt Date: _____

Abstract: We theoretically predict the occurrence of negative differential resistance (NDR) in scanning tunneling spectroscopy (STS) for a pure C_{60} monolayer deposited on a metal surface using metal tips, namely on a Cu(111) surface and using various W tips. It is proposed that the likely reason why NDR has not been observed under such conditions is that NDR can be reduced if an oxidized or Cu-terminated tip is used. A detailed decomposition of the total tunneling current into its contributions from individual molecular orbitals reveals that only some of the orbitals on the tip and on the C_{60} can be "matched up" to give a contribution to the current and that the NDR is a consequence of the mismatch between these specific orbitals within particular ranges of bias voltage. Moreover, the NDR characteristics, including the peak positions and the peak-to-valley ratios, are found to depend on the tip material, tip geometry, and tip-to-molecule position.

PACS: 85.65.+h, 73.61.Wp, 68.37.Ef

I. INTRODUCTION

Negative differential resistance (NDR), defined as a decrease of the electrical current with increasing voltage (within some voltage range), is a key ingredient of molecular electronic devices.[1] Since its realization at the molecular scale in 1999,[2] NDR has drawn considerable attention and has been the subject of many studies.[3-7] Within the context of scanning tunneling microscopy (STM) measurements, including scanning

tunneling spectroscopy (STS), the origin of NDR is generally assigned to the alignment and misalignment in energy of narrow features of both the tip and the sample states as the bias is swept.[8]

C_{60} molecules adsorbed on surfaces have been intensively investigated for their potential applications in molecular electronics. For these, NDR features have been observed in several STM experiments: 1) double- or multi-layers of adsorbed C_{60} molecules;[4] 2) a monolayer of C_{60} molecules on top of an insulator layer;[3,9] and 3) a monolayer of adsorbed C_{60} molecules with reduced molecule-substrate coupling by co-deposition of other molecules.[6,7] So far, no significant NDR has been reported for a pure C_{60} monolayer on a metal surface. For the above three cases, NDR would be favored by the existence of sharp C_{60} molecular levels due to a weak interaction between the substrate and the C_{60}. However, this interaction is strong and broadens[10,11] the molecular levels, thus reducing the possibility for a negative slope in the voltage-current curve, so that it is not surprising that significant NDR features are seldom observed for a pure C_{60} monolayer on metal surfaces.

In the present study, we show that NDR features can in fact be obtained in a pure C_{60} monolayer on a Cu(111) surface through the matching and mismatching between the atomic orbitals (AOs) of the tip apex atom and the molecular orbitals (MOs) of the C_{60} molecule as the bias voltage is changed. The NDR features revealed by theoretical STM and STS simulations is expected to lead to experimental verification. The matching and mismatching between the tip and molecular orbitals with increasing bias voltages are similar to the "local orbital symmetry matching" proposed for the cobalt phthalocyanine (CoPc) molecule with a Ni tip.[5] Furthermore, our results show that the NDR characteristics, including the peak positions and the peak-to-valley ratios, are related to the tip material, tip geometry, and tip-to-molecule position.

II. THEORETICAL MODELING AND RESULTS

Figures 1(a) and 1(b) show the atomic geometry of the C_{60}/Cu(111) adsorption system in one (4x4) unit cell. Based on experimental observations and calculated minimum total energies,[10,12,13] the intact C_{60} molecules are adsorbed on hcp hollow sites of the unreconstructed Cu(111) surface with an orientation illustrated in Fig. 1(b); these form an ordered (4x4) periodic array, as can be prepared and observed experimentally under specific conditions.[12,13] The structure was relaxed (in the absence of a tip) by employing the VASP[14] code based on Density Functional Theory (DFT) at the generalized gradient approximation (GGA) level.[15] In addition, and in order to address the role of the tip in the *I-V* characteristics, we consider different tips, varying both their chemical identity (W, Pt, or Ir) as well as their orientation – see Figs. 2 and 3 for the various tip geometries. We employ the Green's-function-based GREEN code[16,17] for all STM/STS simulations assuming zero temperature. Since the code treats the sample and the tip on an equal footing, it is especially suited for explicitly addressing any tip effects.

We simulate the entire STM system at the atomic level, employing total-energy-optimized geometries for both the sample and the tips.[18] The Hamiltonian of the entire STM system is described with the extended-Hückel theory (EHT),[20] and the EHT-related parameters are obtained after fitting the EHT atom-projected density of states to the *ab initio* counterparts for both the tip and the sample.[18] The EHT parameterization method described in ref. 20 has been proven to yield accurate electronic structures as we fit to the *ab initio* self-consistent results.[17,21] Fig. 1(c) shows the result of the EHT parameterization for the C60/Cu(111) combined system (fitting to the SIESTA atomic projected density of states (DOS)): for fitting the EHT parameters, we divide the C atoms of C_{60} into several groups as a function of their height from the surface, as denoted by C1, C2, C3 and C4 in figure 1(a). The Cu atoms are also divided into several groups: the top layer Cu-1, the in-between layers Cu-fcc and the bottom layer Cu-s. For the top layer Cu-1, the Cu atoms have been further divided into two groups Cu-1a (near to C_{60}) and Cu-1 (far from C_{60}). Fig. 1(c) shows that the *ab initio* atomic projected DOS of the C_{60}/Cu(111) combined system are well reproduced by our EHT parameterization method. The EHT parameters for the various tips are obtained in the same way as described for the sample.

Fig. 2 shows simulated *I-V* curves for C_{60} on Cu(111) with various W tips. In the simulation of the current-voltage (*I-V*) curves, we consider 4 lateral locations of each tip above C_{60}, as shown in Fig. 2(f). In these *I-V* curve plots[22], Negative Differential Resistance occurs whenever such *I-V* curves exhibit a negative slope, e.g. to the high-voltage side of peaks. We consider different tip apex geometries, ranging from a sharp (110)-oriented pyramid to a more blunt (111)-oriented pyramid, as well as a flat (110)-terminated tip obtained by removing the end atom – see insets in Figs. 2(a)-(c), respectively. Since the W tips could be oxidized or pick up a substrate atom very easily, we also simulate W(110) tips with an oxygen or a copper atom at the apex, as shown in Figs. 2(d)-(e). The *I-V* curves in Figs. 2(a)-(c) show that clear NDR features (i.e., negative slopes) are always present with these W tips and for all the tip geometries, regardless whether they are flat or sharp. The NDR peak-to-valley ratios depend on the tip geometry and the tip-to-molecule position. For the flatter W(111) tip, the shape of the *I-V* curves is insensitive to the tip position. Interestingly, Figs. 2(d) and 2(e) show that the NDR is decreased if the oxidized or Cu-terminated W tip is used, suggesting why NDR is rarely observed experimentally despite W tips being often employed: the W tips might be oxidized or pick up substrate atoms during the measurement. Note that the absolute current value depends on the tip-to-molecule position. Generally, the largest current occurs at position 4, while the smallest current occurs at position 3.

Since Pt-Ir alloy tips are also frequently used, we also perform simulations for pure Pt(100) and Ir(111) oriented tips.[23] The simulated *I-V* curves, shown in Fig. 3, reveal that the NDR almost disappears if the Pt(100) tip is used, while it is still present in the case of a very sharp Ir(111) tip, although the occurrence is at a higher sample bias.

From this and other results visible in Figs. 2-3 we may conclude that the NDR features – peak position and peak-to-valley ratio – depend on the tip material, tip geometry, and tip-to-molecule position.

It is known that C_{60} may reconstruct the Cu(111) surface after annealing to well above room temperature.[13,24] Hence we also performed simulations for C_{60} on the reconstructed Cu(111) surface with various W tips. The results (not illustrated here) indicate that, although NDR also appears, the peak-to-valley ratio is smaller than that for C_{60} on the unreconstructed surface. This is due to the fact that the C_{60}-substrate interaction is stronger for C_{60} on the reconstructed surface and hence the broadening in the C_{60} orbitals is larger than that for C_{60} on the unreconstructed surface, reducing the opportunity for negative slopes in the *I-V* curves.

III. MECHANISM OF NDR

To explore the origin of the predicted NDR, we decompose the total tunneling current into its contributions from individual C_{60} MOs and AOs of the last atom of the tip, in order to detect which states contribute most to the current. Since the tunneling current mainly comes from the outermost tip apex atom – for all the simulated tips, we have checked that the apex atom contributes more than 90% of the total tunneling current – we consider only the AO contributions of the tip apex atom in the analysis.

Let us first consider the W(110) tip at position 4 for Figs. 4 and 5. Fig. 4 presents the decomposition into orbitals of the total tunneling current as a function of the applied bias. We include only those states that make a significant contribution. The left panel of Fig. 4 shows that the tip d_{z^2} orbital and, to a lesser extent, the p_z and *s* orbitals contribute significantly to the current. On the other hand, the analysis of the C_{60} MOs reveals that only two relevant sets of orbitals are involved in the tunneling process, corresponding to the lowest virtual (i.e. unoccupied) peaks of the density of states (DOS). In the isolated C_{60} molecule, these sets correspond to unoccupied t_{1u} and t_{1g} orbitals. Upon adsorption on Cu(111), the symmetry is reduced to C_3 and these sets split to A+E orbitals; when taking the tip into consideration, the symmetry is further reduced depending on the tip's own symmetry and position. However the splitting remains modest, especially for that arising from t_{1g}, and participates in the broadening of the DOS peaks in the adsorbed result: it is wider for the lowest peak than for the upper peak. The tunneling involves predominantly the A orbitals, one from each set denoted hereafter LUMOa and LUMOb. The right panel of Fig. 4 shows the contribution of these states to the total current as well as their corresponding wavefunctions.

To interpret the *I-V* characteristics, we adopt the approximation whereby the tunneling current is proportional to the energy-integrated product of the tip's and the molecule's projected densities of states (PDOS), after taking care of the energy shift between the two at each bias.[5] Accordingly, we plot in Figs. 5(a) and (b), respectively, the tip and

molecule PDOS projected onto the states that most significantly contribute to the current. Although the PDOS for the tip p_z orbital is very small, its large spatial extension makes it more accessible to the molecule's states and hence it makes a significant contribution to the current – see Figs. 4(a) and 5(a). For the sake of clarity, we include in Figs. 5(b-d) the combined C_{60} LUMOa and LUMOb PDOS, denoted by "C60-sum".

Once the C_{60} MOs and tip AOs that contribute most to the current are identified, we can determine the origin of the NDR by examining the variation of the alignment between these AOs and MOs at various bias voltages. The NDR appears in the positive sample bias voltage range, for which the tip states shift up in energy relative to the adsorbed C_{60} states. To find the relative energy shift between the PDOS of the tip and of the C_{60} molecule, we fix the energy of the C_{60} LUMOs (LUMOa and LUMOb, combined and denoted by "C_{60}-sum"), while shifting up the energy of the tip AOs with the bias voltage. The NDR appears when the sample bias is larger than 1.3 V. At 1.3 V, the tip d_{z^2} orbital has shifted up in energy by 1.3 eV, as denoted by "1.3 V, tip d_{z^2}" in Fig. 5(c); with even higher bias voltages, the tip d_{z^2} orbital has shifted up further. From Fig. 5(c) we can see that, at bias 1.3 V, in the energy range of 0.0-0.4 eV the broad peak of the tip d_{z^2} orbital matches the broad peak of the C_{60} LUMO. With increasing bias voltage, a mismatch between the two broad peaks appears. At 1.8 V, the broad tip peak is completely mismatched from the C_{60} LUMO. This mismatch between the broad tip peak and the C_{60} LUMO with biases higher than 1.3 V is one source of NDR. In the energy range above 1.1 eV, where the C_{60} LUMOb is located, the tip PDOS decreases with increasing bias voltage: this is another source of NDR.

Thus, with a sample bias larger than 1.3 V, NDR results from the mismatch between the broad peaks of the tip d_{z^2} orbital and of the C_{60} LUMO, and from the decrease of the tip PDOS in the energy range where the C_{60} LUMOb is located. Note that in Figs. 5(c) and (d) we scale the PDOS of the tip and the molecule differently for better visibility. The match and mismatch between the tip *s* orbital and the C_{60} LUMOs are similar to those of the tip d_{z^2} orbital. For the tip p_z orbital with a bias larger than 1.3 V, NDR results from the decrease in the PDOS in the energy region larger than 0.5 eV, as shown in Fig. 5(d).

The same analysis can be applied to the other tips to explain the origin of the NDR features. For the W(111) tip, the tip p_z orbital contributes most to the current, while, for the Ir tip, the tip d_{z^2} orbital contributes most. Figs. 6(a) and (b) show the evolution of the W(111) tip p_z states and Ir tip d_{z^2} states relative to the C_{60} LUMOs. For the W(111) tip with a bias larger than 1.3 V, the NDR resulting from the decrease of the PDOS occurs in the energy region above 0.7 eV. For the Ir tip, the tip d_{z^2} states match the C_{60} LUMOb at 1.8 V, so that the NDR appears at voltages above 1.8 V.

For the C_{60} molecule studied in this work, NDR is significant with a W tip while it

almost disappears for a Pt tip; for the CoPc molecule investigated in previous work,[5] NDR is apparent with a Ni tip but disappears with a W tip; for the terphenylthiol molecule studied in earlier work,[8] NDR appears with a Pt tip. From the NDR behavior discussed in our work and in two previous publications,[5,8] we can draw the conclusion that the occurrence of NDR depends on the electronic structure of both the molecule and the tip. Namely, for a particular molecule, NDR tends to appear only with a suitable tip, depending on the local-DOS peak positions and local orbital symmetries of both the tip and the molecule.

Our work indicates that the occurrence of NDR depends on two factors: a) the relative local-DOS peak position between the tip and the sample; b) the orbital symmetry matching between the tip and the molecule. If one only considers the local-DOS peak position, there are too many peaks in most actual systems. However, if one further considers the orbital symmetry matching between the tip and the sample, we may find that many local-DOS peaks do not contribute to the current. This is the key factor that results in NDR for adsorbed C_{60} with W tips.

IV. CONCLUSIONS

In summary, significant NDR features can be obtained with a pure C_{60} monolayer adsorbed on the Cu(111) surface using various W tips, owing to the match and mismatch between tip AOs and the molecule MOs with increasing biases. NDR is largely insensitive to the tip geometry, which is an important implication for its experimental realization. The easy oxidation and/or pick up of substrate atoms by the W tip, which considerably reduces NDR, would explain why significant NDR has seldom been observed experimentally with W tips, despite the frequent use of such tips. Our findings are expected to be very useful for selecting other tip materials that can present NDR.

Acknowledgments. The work described in this paper is supported by a grant from the Research Grants Council of Hong Kong SAR (project No. CityU 102408) and the Centre for Applied Computing and Interactive Media (ACIM). PWW acknowledges the support from NSC-97-2120-M-002-008-, Taiwan. CM acknowledges the French Consulate in Hong Kong for funding through an exchange program.

References:

[1] R. L. Carroll, and C. B. Gorman, Angew. Chem. Int. Edit. **41**, 4378 (2002).

[2] J. Chen, M. A. Reed, A. M. Rawlett, and J. M. Tour, Science **286**, 1550 (1999).

[3] C. Zeng, H. Wang, B. Wang, J. Yang, and J. G. Hou, Appl. Phys. Lett. **77**, 3595 (2000).

[4] M. Grobis, A. Wachowiak, R. Yamachika, and M. F. Crommie, Appl. Phys. Lett. **86**, 204102 (2005).

[5] L. Chen, Z. Hu, A. Zhao, B. Wang, Y. Luo, J. Yang, and J. G. Hou, Phys. Rev. Lett. **99**, 146803 (2007).

[6] K. J. Franke, G. Schulze, N. Henningsen, I. Fernandez-Torrente, J. I. Pascual, S. Zarwell, K. Ruck-Braun, M. Cobian, and N. Lorente, Phys. Rev. Lett. **100**, 036807 (2008).

[7] I. F. Torrente, K. J. Franke, and J. I. Pascual, J. Phys.: Condens. Matter **20**, 184001 (2008).

[8] Y. Xue, S. Datta, S. Hong, R. Reifenberger, J. I. Henderson, and C. P. Kubiak, Phys. Rev. B **59**, R7852 (1999).

[9] N. A. Pradhan, N. Liu, and W. Ho, J. Phys. Chem. B **109**, 8513 (2005).

[10] L.-L. Wang, and H.-P. Cheng, Phys. Rev. B **69**, 045404 (2004).

[11] F. Schiller, M. Ruiz-Osés, J. E. Ortega, P. Segovia, J. Martínez-Blanco, B. P. Doyle, V. Pérez-Dieste, J. Lobo, N. Néel, R. Berndt, and J. Kröger, J. Chem. Phys. **125**, 144719 (2006).

[12] Tomihiro Hashizume, K. Motai, X. D. Wang, H. Shinohara, Y. Saito, Y. Maruyama, K. Ohno, Y. Kawazoe, Y. Nishina, H. W. Pickering, Y. Kuk, and T. Sakurai, Phys. Rev. Lett. **71**, 2959 (1993).

[13] W. W. Pai, C.-L. Hsu, M. C. Lin, K. C. Lin, and T. B. Tang, Phys. Rev. B **69**, 125405 (2004); W. W. Pai, C. L. Hsu, K. C. Lin, T. B. Tang, Appl. Surf. Sci., 241, 194 (2005).

[14] G. Kresse and J. Furthmüller, Comp. Mater. Sci. **6**, 15 (1996).

[15] J. P. Perdew and Y. Wang, Phys. Rev. B 45, 13244 (1992).

[16] J. Cerdá, M. A. Van Hove, P. Sautet, and M. Salmeron, Phys. Rev. B **56**, 15885 (1997); J. Cerdá, A. Yoon, M. A. Van Hove, P. Sautet, M. Salmeron, and G. A. Somorjai, Phys. Rev. B **56**, 15900 (1997).

[17] http://www.icmm.csic.es/jcerda/.

[18] We used the SIESTA code (Ref. 19) to relax the various tip structures; the EHT parameters are then fitted to the SIESTA atom-projected density of states.

[19] J. M. Soler, E. Artacho, J. D. Gale, A. García, J. Junquera, P. Ordejón, and D. Sánchez-Portal, J. Phys.: Condens. Matter 14, 2745 (2002).

[20] J. Cerdá, and F. Soria, Phys. Rev. B **61**, 7965 (2000) and references therein.

[21] D. Kienle, J. I. Cerdá, and A. W. Ghosh, J. Appl. Phys. 100, 043714 (2006); D. Kienle, K. H. Bevan, G. C. Liang, L. Siddiqui, J. I. Cerdá, and A. W. Ghosh, J. Appl. Phys. 100, 043715 (2006).

[22] In the calculation of the current, the tip-sample vertical distance (perpendicular to the surface) is about 5.2 Å and the maximum absolute current value changes from several tenths of nano-Amperes for the W tips to several nano-Amperes for the Pt tip. Also, the absolute current value depends on the tip-to-molecule position. Generally, the largest current occurs at position 4, while the smallest current occurs at position 3. We have checked that the influence of the distance (from 5.2 Å to 6.2 Å) on the shape of the *I*-*V* curve is not significant.

[23] Since the atomic structure is unknown for Pt-Ir alloy tips, we only simulated pure Pt and pure Ir tips.

[24] Woei Wu Pai et al, to be published.

Figure captions:

Figure 1. (a) and (b) Adsorption geometry of a C_{60} molecule on a (relaxed and unreconstructed) Cu(111) surface, in side (a) and top (b) views; only atoms in one (4x4) unit cell and 4 resp. 1 Cu layers are shown. (c) Atomic projected DOS from SIESTA self-consistent results, compared with corresponding PDOS obtained by fitting EHT parameters to the SIESTA results. The labels refer to atomic layers and groups marked in panel (a); group Cu-1a is shown in yellow, while group Cu-1 is shown in red.

Figure 2. Simulated normalized I-V curves of C_{60} on Cu(111) with various W tips and several tip-to-C_{60} positions (positions 1, 2, 3, and 4 as shown in panel (f)). Side views of the tip geometries are shown in each panel: in panels (a), (b), (d) and (e), the tips are pyramids, the apex atom being mostly responsible for the tunneling; in (c) the apex atom has been removed and the tunneling involves mainly four atoms; in (d) and (e) the apex atom has been replaced by an O and a Cu atom, respectively. Panels (a)-(c) show that NDR occurs prominently with various W tips; panels (d) and (e) show that NDR is weakened with oxidized and Cu-terminated W tips. (f) Empty local-density-of-states image for the adsorption geometry shown in Fig. 1(b). The gray hexagon indicates the top hexagonal ring of C atoms, while numbers denote several lateral tip positions: position 1 places the center of the tip above one C atom, position 2 is over the center of a C-C bridge site, position 3 is over the center of the hexagonal ring, and position 4 is over the brightest point in the image (i.e., over an adjacent pentagonal ring).

Figure 3. Simulated normalized I-V curves of C_{60} on Cu(111) for a Pt(100) tip (left) and an Ir(111) tip (right) for various tip positions, as labeled in Fig. 2(f).

Figure 4. The total tunneling current decomposed according to the atomic orbitals of the tip apex atom (left) and the molecular orbitals of C_{60} (right); the corresponding molecular orbital wave-functions are also shown.

Figure 5. (a) and (b): PDOS of the tip apex AOs and the C_{60} MOs, resp., that significantly contribute to the current (the small p_z PDOS values are magnified in the inset); the Fermi energy is set to zero; (c) and (d): evolution of tip d_{z^2} and p_z orbitals, resp., relative to the C_{60} LUMOs, with increasing sample biases of 1.3 and 1.8 V. “C60-sum” denotes LUMOa and LUMOb combined.

Figure 6. The up-shift of the W(111) tip p_z states (a) and the Ir tip d_{z^2} states (b) relative to the C_{60} LUMOs with increasing bias voltages. See Fig. 5 for more details.

Figure 1.

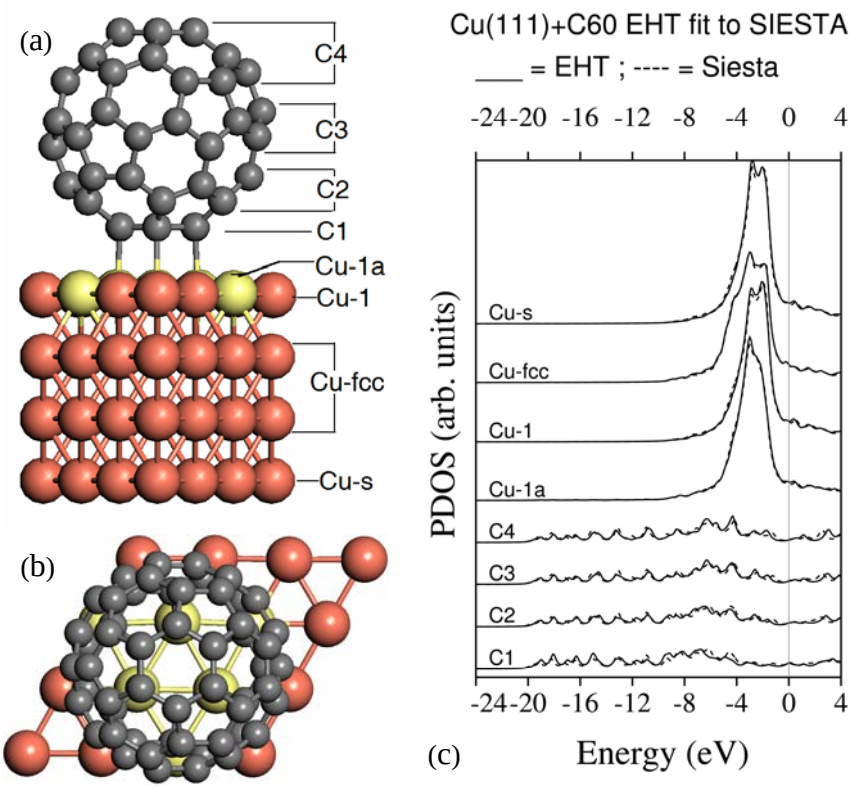
(a)
C4
C3
C2
C1
Cu-1a
Cu-1
Cu-fcc
Cu-s
(b)
Cu(111)+C60 EHT fit to SIESTA
___ = EHT ; ---- = Siesta
-24 -20 -16 -12 -8 -4 0 4
PDOS (arb. units)
Cu-s
Cu-fcc
Cu-1
Cu-1a
C4
C3
C2
C1
-24 -20 -16 -12 -8 -4 0 4
(c)
Energy (eV)

Figure 2.

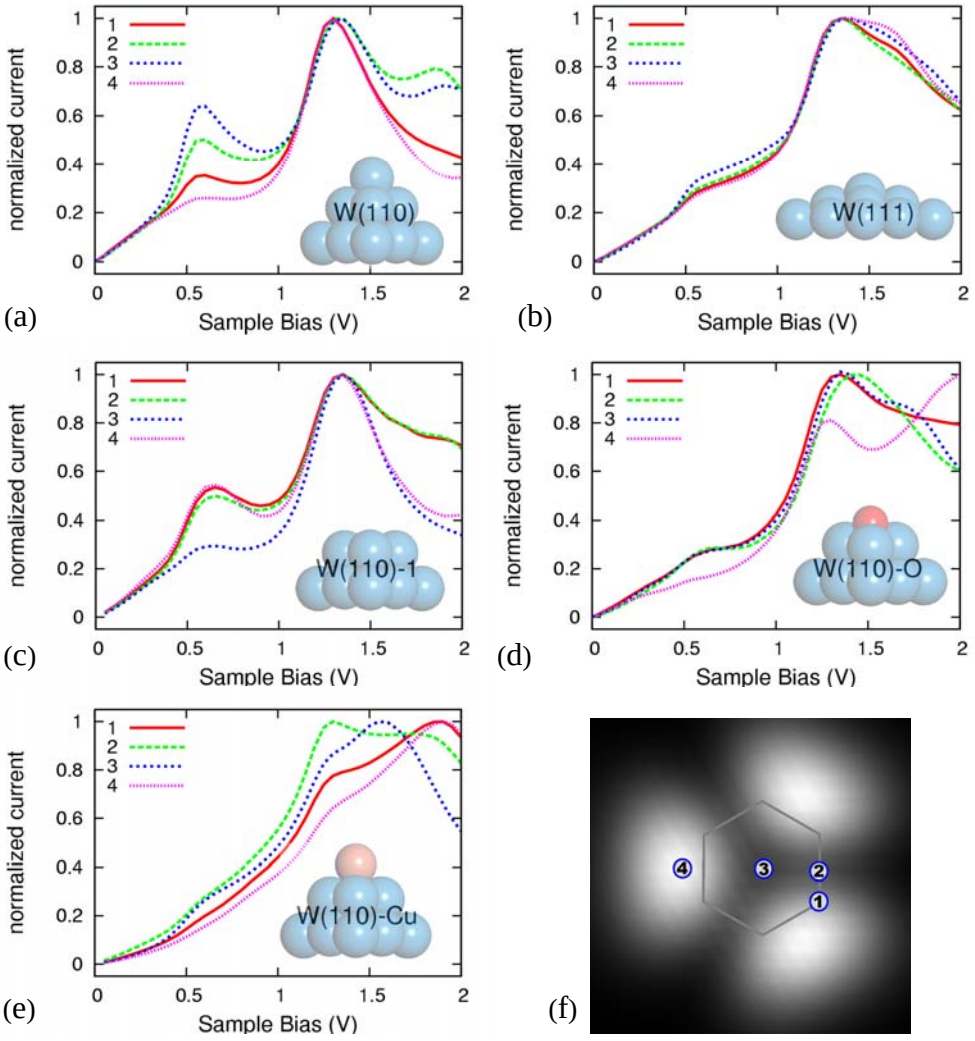
normalized current
Sample Bias (V)
1
2
3
4
W(110)
(a)
W(111)
(b)
W(110)-1
(c)
W(110)-O
(d)
W(110)-Cu
(e)
(f)

Figure 3.

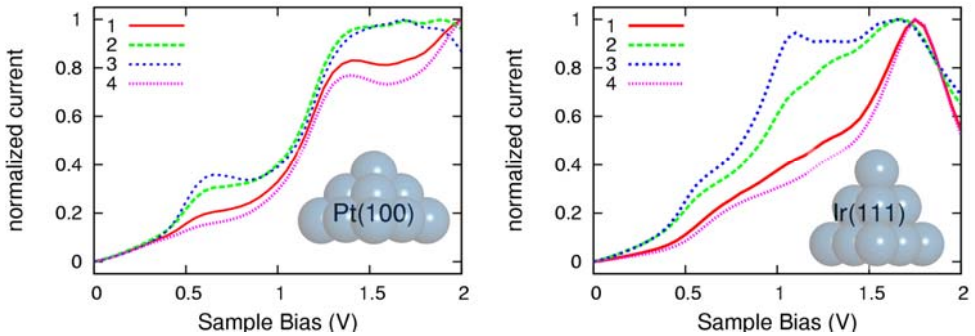

Figure 4.

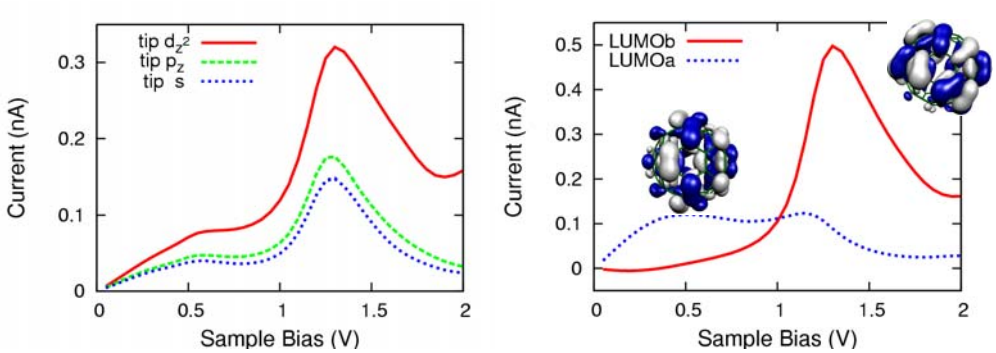
tip d_{z^2}
tip p_z
tip s
Current (nA)
Sample Bias (V)
LUMOb
LUMOa
Current (nA)
Sample Bias (V)

Figure 5.

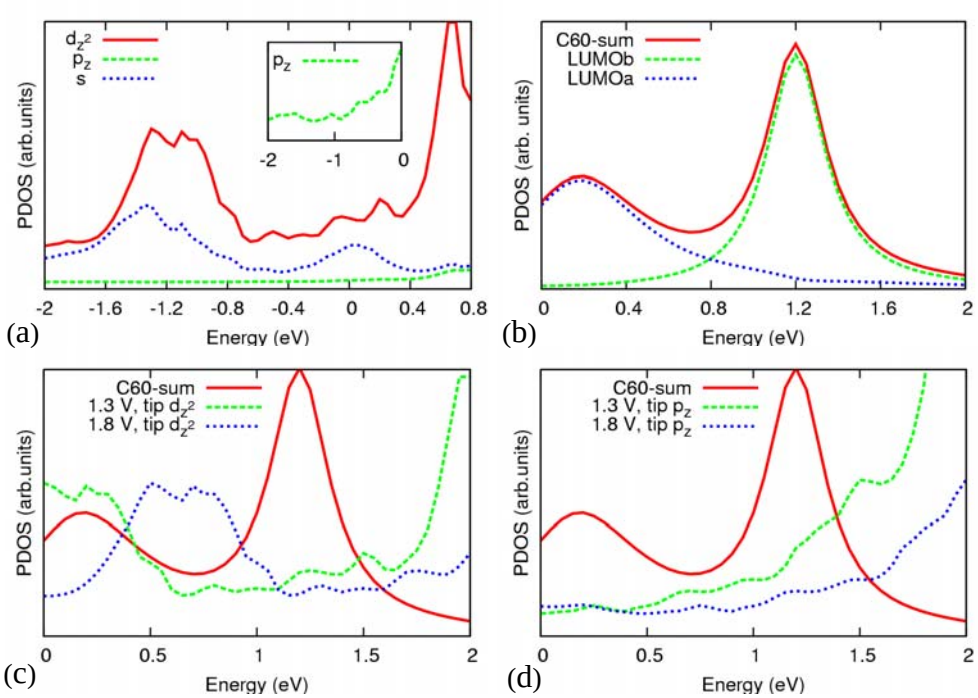
(a)
PDOS (arb.units)
Energy (eV)
d_{z^2}
p_z
s
p_z
-2
-1
0
-2
-1.6
-1.2
-0.8
-0.4
0
0.4
0.8
(b)
PDOS (arb. units)
Energy (eV)
C60-sum
LUMOb
LUMOa
0
0.4
0.8
1.2
1.6
2
(c)
PDOS (arb.units)
Energy (eV)
C60-sum
1.3 V, tip d_{z^2}
1.8 V, tip d_{z^2}
0
0.5
1
1.5
2
(d)
PDOS (arb.units)
Energy (eV)
C60-sum
1.3 V, tip p_z
1.8 V, tip p_z
0
0.5
1
1.5
2

Figure 6.

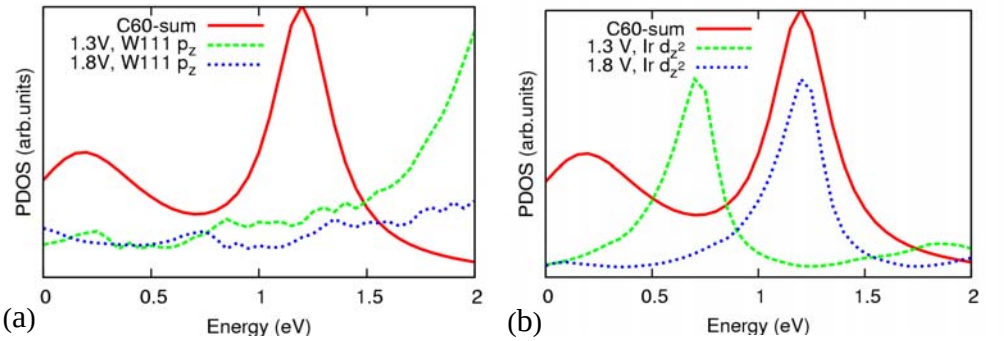
C60-sum
1.3V, W111 p_z
1.8V, W111 p_z
PDOS (arb.units)
0
0.5
1
1.5
2
Energy (eV)
(a)
C60-sum
1.3 V, Ir d_{z^2}
1.8 V, Ir d_{z^2}
PDOS (arb.units)
0
0.5
1
1.5
2
Energy (eV)
(b)